Base suction, entrainment flux, and wake modes in the vortex formation region at the rear of a three-dimensional blunt bluff body

Laurent Keirsbulck [1,2,*], Olivier Cadot,[3] Jérémy Basley [1,2] and Marc Lippert [1,2]

[1] *Univ. Polytechnique Hauts-de-France, F-59313 Valenciennes, France*
[2] *LAMIH, UMR 8201 CNRS, F-59313 Valenciennes, France*
[3] *School of Engineering, University of Liverpool, United Kindgom*

A slitted base cavity of constant depth with a varying filling ratio $0 \leqslant R_f \leqslant 100\%$ is experimentally investigated to reduce the form drag of a three-dimensional blunt body (the so-called squareback Ahmed body) at a Reynolds number $\mathrm{Re} = 2.89 \times 10^5$. The drag reduction is achieved by a decrease of base suction (or, equivalently, the increase of pressure at the base). The plain cavity ($R_f = 100\%$) reduces the base suction by 22% compared to the case with no cavity ($R_f = 0$). All intermediate filling ratio are obtained by the enlargement of the slits, initially having a zero width for the plain cavity case. It is shown that the gradual base suction change can be related to the level of the entrainment flux of the free shear layers developing from the rear separation and to the suppression of the transverse steady asymmetric instability of the wake. The model of the vortex formation region length of Gerrard [J. Fluid Mech. **25**, 401 (1966)] is shown to provide an insightful interpretation of the drag reduction mechanism using ventilated base cavities.

I. INTRODUCTION

Gerrard [1] proposed in 1966 the mechanics of the formation region of vortices behind bluff bodies produced by the rear flow separation (see Fig. 1). This model explains the monotonous drag increase over almost two decades of Reynolds number (Re) before the spectacular transitions of the drag crisis observed for an incompressible flow past bodies with smooth separations. The corresponding range is $\mathrm{Re} \approx 2 \times 10^3$–$2 \times 10^5$ for the cylinder where the drag coefficient increases approximately from 1 to 1.3 (see, for instance, Schlichting and Gersten [2]). This increase, related to a wake effect, is particularly noticeable in the base suction plot by Roshko [3]. Gerrard [1] interpreted the wake effect as a modification of the equilibrium in the volumetric fluxes filling and emptying the vortex formation region. The modification is related to the transition to turbulence of the laminar free shear layers initiated at the separation. The transition, that appears locally in the free shears, thus produces a global effect on the recirculating length responsible for the drag modification as described in the following. Let us define first ψ as the total volumetric flux entrained by the shear layers in the formation region. This entrainment is produced by the growth rate of the developing free shears (see, for instance, Schlichting and Gersten [2]). Flux ψ depicted in Fig. 1 thus evacuates downstream the formation region some fluid from inside the mean recirculating bubble. Since the laminar to turbulent transition location in a free shear moves upstream as Re increases, the turbulent portion of the shear layers in the formation region gets elongated. Knowing that the total entrainment flux increases with the turbulent shear length, ψ in Fig. 1 consequently increases as the Reynolds number is increased. This mechanism is continuous until the transition is close enough to the body wall to provoke either a massive reattachment for bodies of smooth separation (the drag crisis transitions [4]) or a saturation of the formation length for bodies with a salient separation (the case of blunt base geometry). The assumption of Gerrard [1] considers the formation region closure as governed by inviscid instabilities that, as such, related in-flux Φ_{in} and out-flux Φ_{out} in Fig. 1 remain unchanged as Re increases and the same for the entrainment flux since $\psi = \Phi_{\mathrm{in}} - \Phi_{\mathrm{out}}$ when the formation region is at the equilibrium. Thus, the new equilibrium is only made possible with a shorter formation length, having shorter turbulent shear layers to keep ψ constant.

The unambiguous relationship between the inverse of the formation length and base suction has been demonstrated by Bearman [5] with base bleed control of a "D" shape cylinder. The correlation is theoretically supported by the inviscid cavity models [6], where the cavity denotes the dead zone of no fluid motion. These models establish a general behavior of base suction [3] (defined as minus the pressure difference between the pressure inside the cavity and the free stream pressure) evolving as positive power laws of the inverse of the cavity length whatever the cavity closure model used. Physically, the high base suction is produced by the flow curvature around the cavity. For viscous wake flows at large Reynolds number, this trend still remains, with the recirculating bubble playing the role of the cavity [3]. The shorter the formation length or the recirculating bubble the higher the base suction.

Gerrard's model [1] has been successfully used with an additional influx produced by base blowing [7]. This experiment
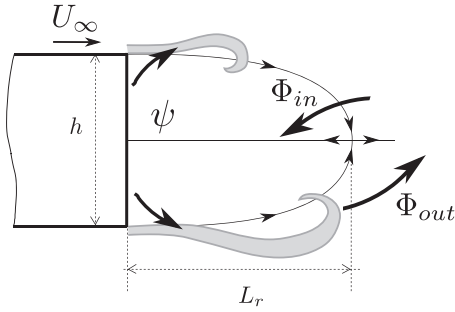
*laurent.keirsbulck@uphf.fr

FIG. 1. Schematic view of the vortex formation region at the rear of a blunt base body. Gray shapes are representing instantaneous free shear layers and the background streamlines show the mean recirculating bubble of length L_r. Thick arrows depict volumetric fluxes of the formation region as defined by Gerrard [1]: entrainment flux ψ by the free shear layers, in-flux Φ_{in} and out-flux Φ_{out} at the vortex formation closure.
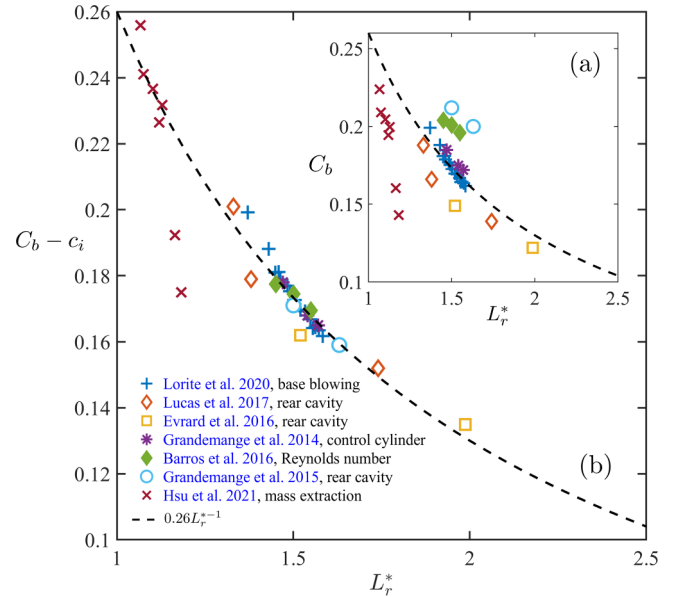

FIG. 2. Base suction compilation from literature for a flat-back Ahmed body under different controls as a function of the recirculation bubble length (a). In (b) the same experimental data sets are shifted vertically by a constant value c_i (see text).

considers the flow past a three-dimensional (3D) blunt base rectangular body (the so-called squareback Ahmed body [8]). The Gerrard's formation length model explains the equilibrium bubble size and the associated drag reduction in, as referred by the authors [7], the "mass regime" where the blowing momentum flux is negligible or equivalently previously known as drag reduction with base bleeding [9]. A similar relationship for the squareback Ahmed body as for the "D" shape cylinder of Bearman [5] is also observed between the equivalent of the formation length, the bubble length [that can now be measured using particle image velocimetry (PIV)] and the base suction. Variations of the bubble length have been achieved in different ways in the recent literature of the squareback Ahmed body using control cylinders [10], rear cavities [11–13], base blowing using different gaz densities [7,14], and base flow extraction [15] and also by changing the Reynolds numbers [16]. The reported bubble lengths L_r^* in Fig. 2(a) are displayed in unit of the body height h and have been measured using PIV in a vertical central plane except for Hsu *et al.* [15] where the plane is horizontal and at a distance $h/4$ below the top of the body. All the experiments show a same trend: The shorter the bubble length, the larger the base suction but with vertical shifts between the data sets. As the base suction coefficient is defined from a reference pressure that might differ from one author to another, we have artificially shifted each data set by a constant base suction c_i to obtain the best superimposition with the data of Lorite-Díez *et al.* in Fig. 2(b). We can see a trend $C_b - c_i = 0.26 L_r^{*-1}$, where c_i is the constant value relative to each experimental data set "i." The discrepancy with the data of Hsu *et al.* [15] can reasonably be attributed to the different location of the bubble size measurements. Figure 2(b) shows that the bubble size is an indicator of the squareback Ahmed body drag. The bubble size depends on the entrainment flux carried out by the turbulent shear layers in the formation region.

The vortex formation region closure involves complex turbulent dynamics. While it is essentially dominated by the vortex shedding (Bénard von Kármán instability) for two-dimensional bodies [1,3], there is less consensus for three-dimensional bluff bodies. The most recent investigations

on azimuthal wake modes m of blunt base axisymmetric bodies [17–23] report the presence of an antisymmetric $m = 1$ periodic mode associated with vortex shedding, symmetric $m = 0$ disturbances related to pumping or breathing motion of the formation region and a steady $m = 1$ mode responsible for very low frequency stochastic dynamics. It is quite similar for squareback geometries [24–30], except that two periodic modes $m = 1$ are reported and that the very low frequency stochastic dynamics associated with the steady $m = 1$ mode are restricted to bistable dynamics. It has to be mentioned that the $m = 1$ steady and periodic modes are reminiscent of the first and second bifurcation respectively in the laminar regime of both the axisymmetric [31,32] and squareback [33,34] geometries.

The base cavity formed by additional walls at the rear of the model, that is considered in the paper, is known to be an efficient drag reducer device of blunt base bodies [9] by decreasing the base suction. In addition, Morel [35] reported almost no change in the $m = 1$ global mode frequency of the axisymmetric body with a base cavity. A similar conclusion is also made by Lorite-Diez *et al.* [36] for the squareback Ahmed body. On the other hand, the steady asymmetric mode $m = 1$ for both axisymmetric and squareback geometries is found to be totally suppressed [11,12,37,38] for base cavities deeper than 25% the body height.

The aim of the paper is to investigate directly the sensitivity of the base suction of a squareback Ahmed body to the entrainement flux ψ as depicted above and in Fig. 1. Experimentally, the original idea is to mitigate the flux with additional solid walls extending downstream from the base and forming a slitted base cavity as shown in Fig. 3. A simple physical model derived from the formation region budget of Gerrard will relate the base suction directly to both the mitigation of the entrainment flux ψ and the stabilization of the
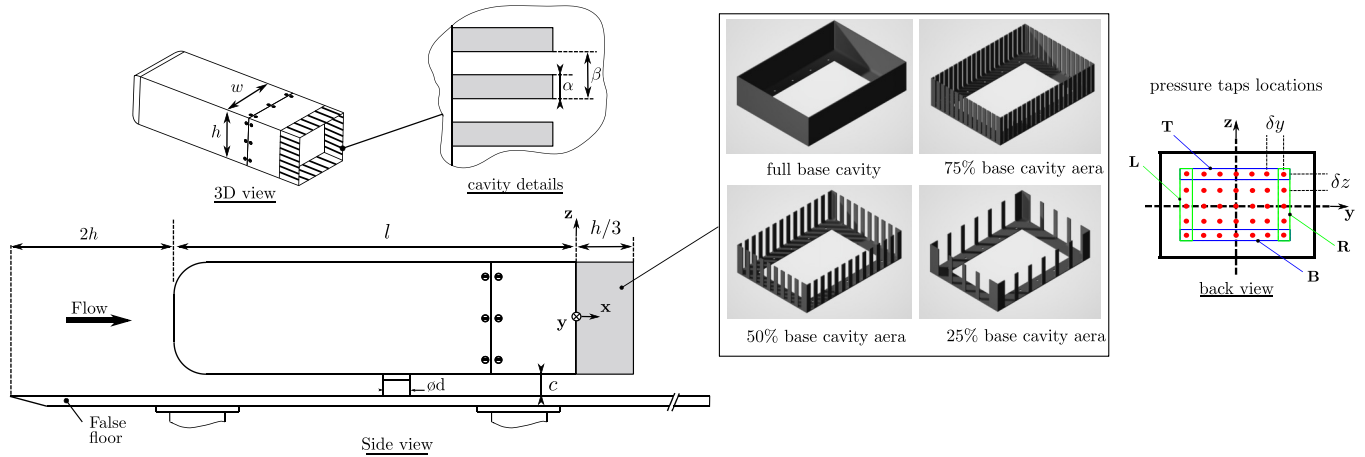
FIG. 3. Setup and base cavity geometry parameters.

steady asymmetric mode. The paper is outlined as follows. The experimental setup is detailed in Sec. II. Section III is devoted to the analysis of the results. In particular, the base pressure drag behavior is discussed with regards to the steady asymmetric mode followed by a focus on the two periodic modes evolution. An extension of the mass regime model of Lorite-Díez *et al.* [7] inspired from Gerrard [1] is finally introduced and discussed in Sec. IV before conclusions in Sec. V.

II. EXPERIMENTAL SETUP AND CAVITY BASE GEOMETRIES

The present experiment was performed in the Lamih closed-circuit subsonic wind tunnel with a 6.25:1 contraction ratio. The 10-m-long working section has a 2×2 m^2 cross-sectional area and the free-stream turbulent intensity is less that 0.6%. The Ahmed body model shown in Fig. 3 was centered between the side walls, the ceiling, and the floor within the test section. The geometry is placed in wall proximity with a plate up-raised from the wall of the tunnel. The coordinate system is defined as **x** in the streamwise direction, **z** normal to the ground, and **y** in the lateral direction as shown in Fig. 3. The bluff body geometry has a width (w) of 272 mm, a height (h) of 202 mm, and a length (l) of 730 mm, and the cylindrical central support has a diameter of 50 mm. The ground clearance of the geometry, denoted by c, is set to 42 mm. The model without the support corresponds to the original Ahmed body [8] configuration with a scale of 0.7. Based on the height of the model, the Reynolds number of this flow is defined as $\text{Re}_h = U_\infty.h/\nu$, where ν is the kinematic viscosity of the air at ambient temperature and U_∞ the free-stream velocity. Experiments are conducted for a free stream velocity U_∞ of 21.5 m/s, corresponding to $\text{Re}_h = 2.89 \times 10^5$. Note that in the following, the superscript * denotes the nondimensional value by using h, U_∞. Instantaneous quantities are denoted with lowercase letters (e.g., g_y, c_b), their time average with uppercase letters (e.g., G_y, C_b), and their standard deviation with primed uppercase letters (e.g., G'_y, C'_b). Also, #**P** and #**N** denote the positive and negative states of the steady asymmetric **y** instability.

The pressure is measured at 35 locations at the back of the body as shown in Fig. 3. The pressure taps are equally spaced with distances $\delta y^* = 0.15$ in the **y** direction and $\delta z^* = 0.12$ in the **z** direction. The static pressure is measured with a miniature Scanivalve Mps4264 pressure scanner. The instantaneous pressure coefficient is computed by:

$$c_p(t) = \frac{p(t) - p_\infty}{p_{\text{dyn}}}$$

with $p_{\text{dyn}} = \frac{1}{2}\rho U_\infty^2$ and where ρ denotes the air density and p_∞ the reference static pressure, measured at the side-wall of the test section, aligned with the front of the body. The base suction coefficient c_b is computed from the spatial average of the 35 pressure taps at the base:

$$c_b(t) = -\frac{1}{35}\sum_{i=1}^{7}\sum_{j=1}^{5} c_p(y_i, z_j, t).$$

The pressure scanner is located inside the model so that it is linked to each tap with less than 150 mm of vinyl tube to limit the filtering effect of the tubing leading to a natural low-pass filtering having a cutoff frequency approximately 150 Hz ($f_c^* = 1.41$). The accuracy of the pressure scanner (effective measurement range of 2000Pa) is given by the manufacturer to be $\pm 0.15\%$ fso corresponding to ± 3Pa. However, converged time-averaged values have a better accuracy that falls below [39] ± 0.5Pa. So the accuracy in terms of mean base suction coefficients is ± 0.001. The 35 pressure channels are recorded during 300 s to ensure good statistical convergence at a sampling frequency of 850 Hz per channel. The wake asymmetry is assessed by using the dimensionless horizontal and vertical base pressure gradients, g_y and g_z. The four pressure taps group (**L**, **R**, **T**, **B**) indicated in blue and green in Fig. 3 are used to compute the base pressure gradient components:

$$g_y = \frac{\langle c_p \rangle_{\mathbf{R}} - \langle c_p \rangle_{\mathbf{L}}}{6\delta y^*}, \quad g_z = \frac{\langle c_p \rangle_{\mathbf{T}} - \langle c_p \rangle_{\mathbf{B}}}{4\delta z^*},$$

with $\langle . \rangle_n$ denoting the spatial average of the taps group n. The gradient components are low pass filtered with moving window of 50 ms just for the time history representations for clarity.
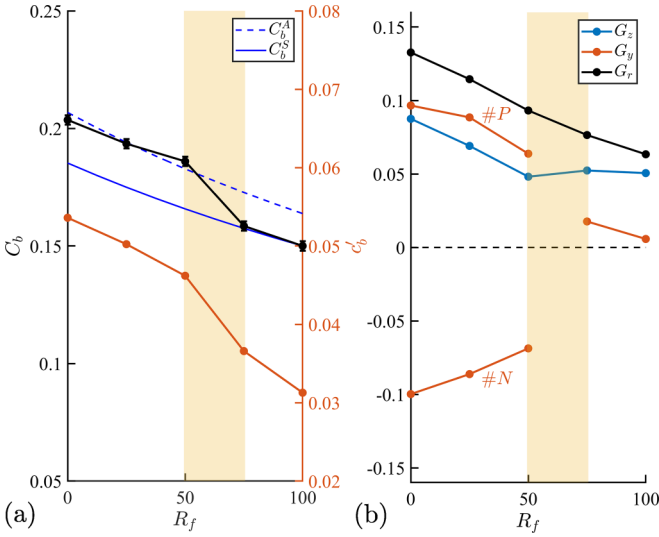
FIG. 4. Mean and fluctuation of the base suction coefficients (C_b and c_b') (a) and mean pressure gradient components (G_y, G_z, and G_r) against cavity ratio R_f (%) (b). The blue dashed and continuous lines are an entrainment mitigation flux model for the base suction, $C_b^A = 0.26(L_{r_0}^{*A} + d^* \cdot R_f)^{-1}$ and $C_b^S = 0.26[L_{r_1}^{*S} + d^*(R_f - 1)]^{-1}$, respectively, where $L_{r_0}^{*A} = 1.26$ and $L_{r_1}^{*S} = 1.74$ (see text).

Various base cavities of depth $d^* = 0.33$ and thickness $e^* = 0.01$ (Fig. 3), are implemented at the rear of the reference model to evaluate their effect on the turbulent wake behind the body. The base cavities have various surfaces filling coefficient defined as $R_f = \alpha/\beta$, where $\alpha^* = 0.05$ and β^* are the characteristic lengths reported in Fig. 3. The depth $d^* = 0.33$ has been chosen because, as shown by Evrard *et al.* [11], it achieves a full stabilization of the steady asymmetric mode for the plain cavity ($R_f = 100\%$). All parts are 3D printed with an ultimaker F5. After printing, a glossy primer is applied with a fine finish to achieve a surface roughness of approximately 0.1 mm. Four different configurations of base cavities in addition to the reference case are defined.

III. RESULTS

A. Base suction

The mean base suction is shown in Fig. 4(a) as a function of the cavity filling coefficient. Compared to the squareback reference ($R_f = 0\%$), a base suction reduction of 22.4% is obtained with the plain cavity ($R_f = 100\%$) in agreement with the typical reduction of about 20% reported previously by Evrard *et al.* [11] (17.8%), Lucas *et al.* [12] (26.1%), Lorite-Diez *et al.* [36] (24%), and Bonnavion and Cadot [40] (25%). The reduction continuously decreases as the cavity filling coefficient increases. The decline is fairly constant before 50% and jumps to a lower value between 50% and 75%, outlined with the yellow stripe in Fig. 4. The fluctuation of the base suction follows the same trend.

B. Steady global mode

The permanent asymmetry of the wake due to the steady asymmetric **y** instability [17] is directly observable in the

time series of the horizontal base pressure gradient in Fig. 5 that alternatively switches between two opposite values characteristic of the **#P** and **#N** states of the wake. These two asymmetric mirrored states will be referred to as the steady mode for the remainder of the paper. Their corresponding averages conditioned by the sign of g_y for filling coefficients $R_f \leqslant 50\%$ are reported in Fig. 4(b). From $R_f = 75\%$, it becomes impossible to distinguish between the two states, as can be seen in the time series of Fig. 5. Fluctuations of horizontal gradient component are drastically reduced and g_y remains close to zero. This indicates the suppression or stabilization of the steady mode. The asymmetry of the wake can be measured by the mean of the instantaneous modulus of the gradient, G_r, that is displayed in Fig. 4(b). It shows a monotonous decrease and keeps a large value even for the stabilized wake at $R_f = 100\%$; this is essentially due to the permanent vertical component produced by the floor. The inhibition of the steady mode can be also assessed by the power spectrum density (PSD) of g_y shown in Fig. 5 for the five filling ratios. The gradual disappearance of the low frequency contribution is the simple consequence of the switch amplitudes that tend to zero when the wake is stabilized. The stabilizing effect observed here as the filling coefficient is increased is likely similar to the case reported by Evrard *et al.* [11], in which the cavity depth increases with a constant filling coefficient of 100%. The vertical component of the gradient also decreases continuously with R_f as in Evrard *et al.* [11] with the cavity depth leading to a centering of the base pressure distribution of the stabilized wake.

The pressure imprint of the spatial structure of the steady mode for the reference ($R_f = 0\%$) can be observed in Fig. 6(a) where the statistics are conditioned by the positive base pressure component $g_y > 0$ to display the **#P** state of the wake. The same structure is observed in Fig. 6(b) for half-filled cavity ($R_f = 50\%$) but attenuated. The plain cavity displays a rather symmetric distribution in conformity to previous works [11,12,38]. The presence of the steady mode is responsible for the clear asymmetry of the base pressure fluctuations in Figs. 6(a) and 6(b). The quasisteady left part of the **#P** state coincides with the recirculating torus [12] nestled against the base. The frequency content of the pressure fluctuations is discussed in the next section.

To summarize, the sudden decrease of base suction and of its fluctuation highlighted by the yellow stripe in Fig. 4 is unambiguously correlated to the stabilization of the steady mode as the filling ratio is increased.

C. Unsteady global modes

The two antisymmetric periodic global modes are identifiable in the PSD of the base pressure gradient components for the squareback reference in Fig. 5. There is a well-defined concentration of energy around $f^* = 0.185$ in the PSD of the vertical component and around $f^* = 0.135$ for the horizontal component. These frequencies are very close to values reported in the literature for identical base aspect ratio Ahmed body [7,15,24,25,29]. It is commonly reported that the antisymmetric global mode frequency is related to the separating distance between a pair of facing interacting free shears, where the closer the shear, the higher the frequency similarly
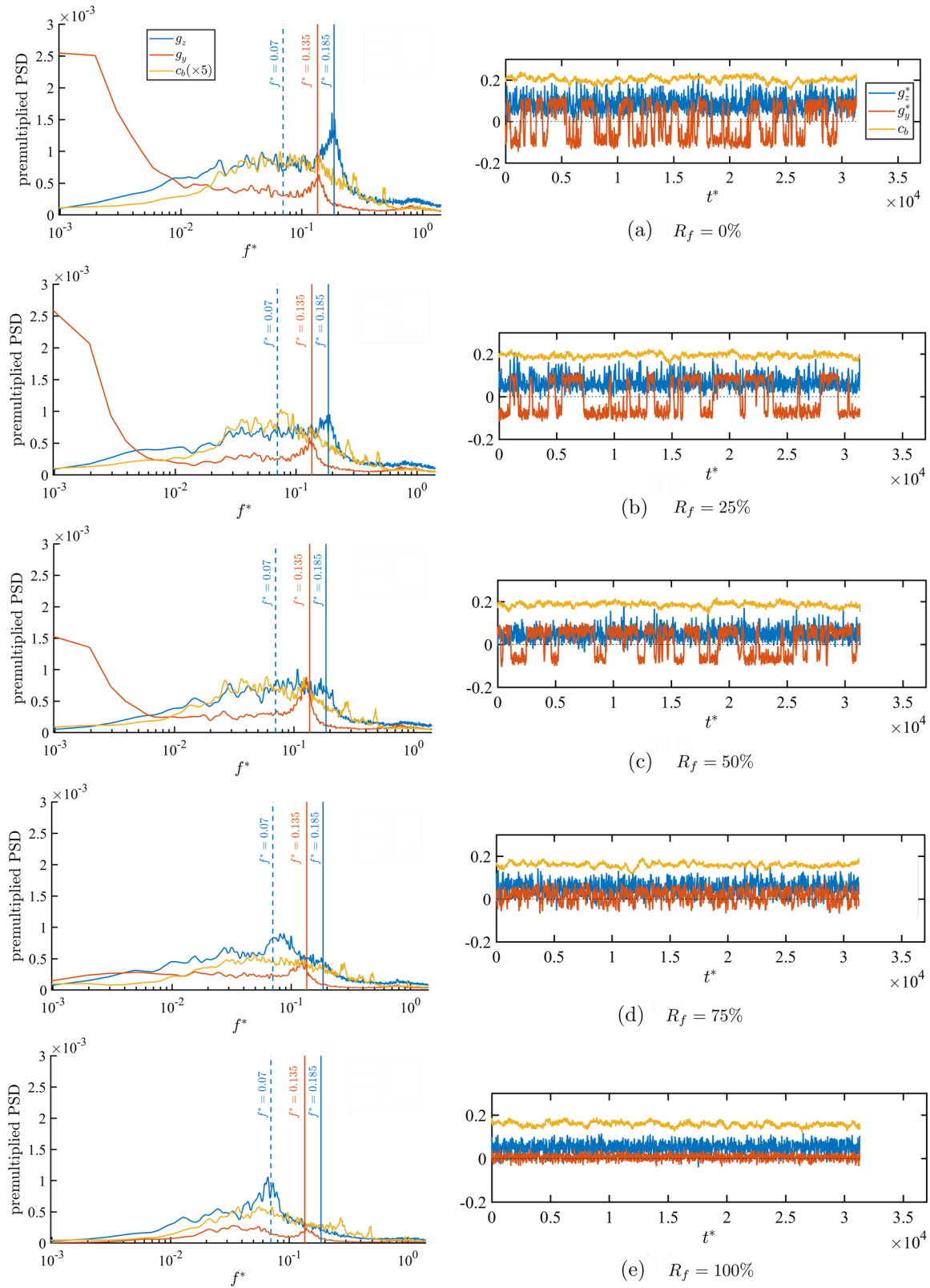
FIG. 5. Time histories and power spectral densities of the pressure gradients, g_y and g_z, and of the base pressure coefficient, c_b, are plotted for the five R_f ratios (a) to (e).
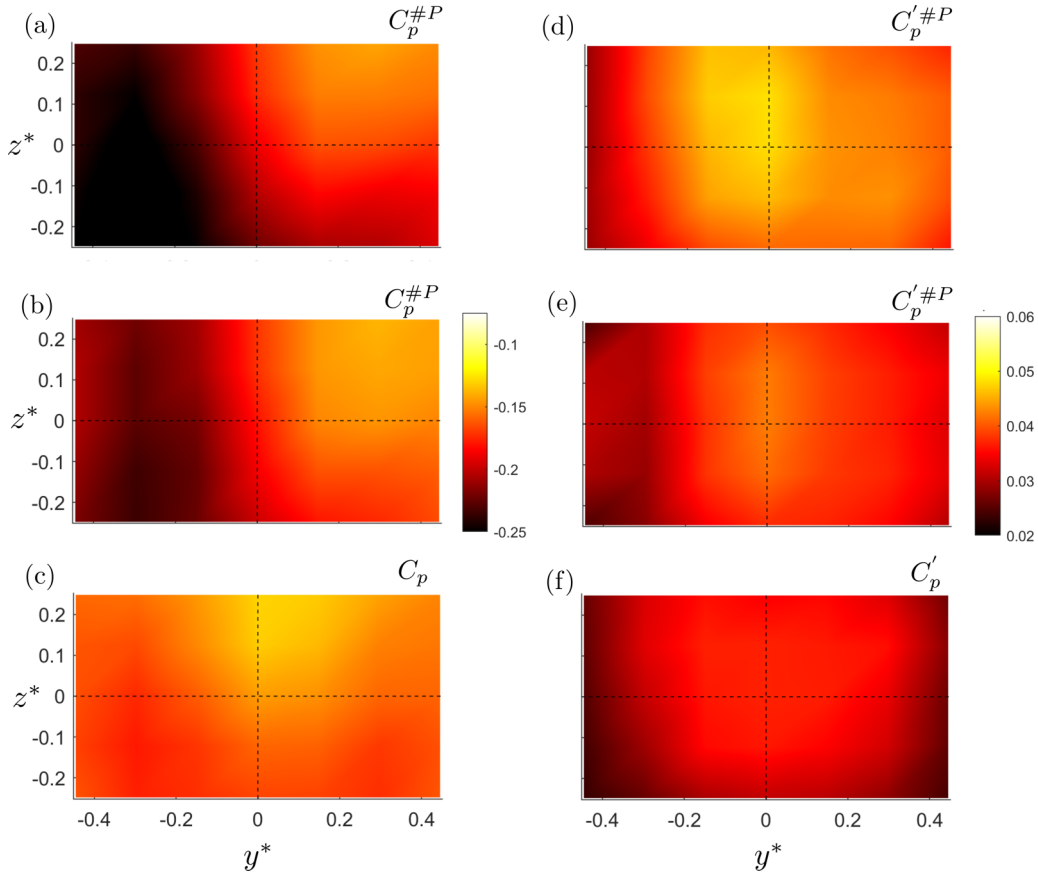
FIG. 6. Mean and fluctuation of the pressure coefficient distribution at the base of the body; for $R_f = 0\%$ [(a) and (d)], $R_f = 50\%$ [(b) and (e)], and $R_f = 100\%$ [(c) and (f)]. The two first case refer to as to the positive state #**P**.

to the vortex shedding mode of cylinder flow [3,41]. These separating distances are here the base height and width of the rectangular base, thus leading to a higher frequency of the oscillations in the z direction that in the y direction. However, Kiya and Abe [42] have showed that the ratio of the separating distances does not simply equal that of the frequencies.

The peak at $f^* = 0.135$ found in the horizontal gradient component g_y seems to persist for all cavity filling ratios, although with small variations in amplitude and peak frequency. The peak at $f^* = 0.185$ in the vertical gradient component g_z disappears in the background noise from $R_f = 50\%$ on. This might not necessarily imply the stabilization of the corresponding periodic wake mode. As reported by Varney [38] the dead zone of motion at the bottom of the deep cavity damps the antisymmetric pressure disturbances coming from downstream, where the wave maker of the periodic wake modes is located. In addition, Lorite-Diez et al. [36] did not obtain any change in the vertical oscillation of the wake mode using hot-wire anemometry with a deep cavity. However, new dynamics appear unambiguously with a peak emerging around $f^* = 0.07$ from $R_f = 75\%$ on. This antisymmetric mode could be related to an instability of the feedback flow interacting with the cavity walls.

Symmetric global modes can be observed from the PSD of $c_b(t)$, corresponding to the mode 0 deformation of the pressure distribution. No specific energy peak can be singled out from Fig. 5 at any filling ratio. There is then no identifiable mode associated with a specific scale for symmetric disturbances

but rather a continuum spread around $f^* = 0.07$. The corresponding global dynamics is generally related to a breathing or pumping motion of the recirculating region.

IV. DISCUSSION

A. Entrainment mitigation flux model

As originally proposed by Lorite-Díez et al. [7], and referred to as "mass regime," the equilibrium of the volumetric flux across the recirculation bubble can be written as:

$$\Phi_{\text{out}} + \psi = \Phi_{\text{in}} + q_m, \quad (1)$$

where ψ, Φ_{out}, and Φ_{in} are the same fluxes as those defined in Fig. 1 and q_m is an additional source of negligible momentum introduced through base bleeding in Lorite-Díez et al. [7]. The entrainment flux carried out by the free shear layers ψ can be evaluated [7] as $\psi = v_e\, l\, L_r$, with v_e, l, and L_r being the entrainment velocity, the peripheral length of the mixing layers [here roughly $2(w + h)$], and the length of the free shears in the formation region given by recirculation length. As the free shear layers are turbulent for the considered Reynolds number, the entrainment velocity is constant and thus independent of the location in the developing free shears. If the fluxes Φ_{out} and Φ_{in} at the bubble closure remain insensitive to the additional source, then Eq. (1) applied to the natural case ($q_m = 0$, denoted in the following with a subscript 0), $\Phi_{\text{out}} + \psi_0 = \Phi_{\text{in}}$, gives $\psi - \psi_0 = q_m$, and the resulting recirculation length of the mass regime equilibrium reads with the additional source

q_m:

$$L_r = L_{r_0} + \frac{q_m}{v_e l}. \tag{2}$$

In the present experiments there is no additional source feeding the formation region, $q_m = 0$, but the entrainment flux is mitigated by the extended walls of length d and filling ratio R_f. We derive a simple relationship by setting to zero the entrainment velocity at any locations of the extended walls such that the entrainment flux reduces to:

$$\psi = v_e l L_r - v_e l R_f d. \tag{3}$$

If the fluxes Φ_{out} and Φ_{in} at the bubble closure remain insensitive to the entrainment mitigation, then $\psi = \psi_0$ and we obtain a same expression as in Eq. (2) with an equivalent additional source $q_m = v_e l R_f d$. This source can be seen as the flux that is not entrained by the free shears due the presence of the extended walls.

As concluded in Sec. III B, the jump in C_b observed in Fig. 4(a) is due to the stabilization of the steady asymmetric wake mode. The stabilization modifies the bubble closure dynamics and, consequently, the in-flux $\Phi_{\text{in}} - \Phi_{\text{out}} = \psi_{\text{in}}$ of the formation length budget. To account for this modification, two models for the bubble length are derived as a function of the filling ratio R_f. The first model, referred to as the asymmetric model denoted with superscript A, accounts for a bubble closure dynamics as observed for $R_f = 0$. The second model, referred to as the symmetric model denoted with superscript S, accounts for a bubble closure dynamics as observed for $R_f = 100\%$. For each model the in-flux ψ_{in} remains constant but has different value depending on the closure dynamics, $\psi_{\text{in}}^A \neq \psi_{\text{in}}^S$. The asymmetric model is derived as follows:

$$\psi^A = v_e l L_r^A - v_e l R_f d = \psi_{\text{in}}^A$$
$$\psi_0^A = v_e l L_{r0}^A = \psi_{\text{in}}^A, \tag{4}$$

leading to

$$L_r^A = L_{r0}^A + R_f d. \tag{5}$$

The symmetric model is derived as

$$\psi^S = v_e l L_r^S - v_e l R_f d = \psi_{\text{in}}^S$$
$$\psi_1^S = v_e l L_{r1}^S - v_e l d = \psi_{\text{in}}^S, \tag{6}$$

leading to

$$L_r^S = L_{r1}^S + (R_f - 1) d. \tag{7}$$

For both models, subscripts 0 and 1 refer respectively to values at $R_f = 0$ (natural case) and $R_f = 100\%$ (plain cavity). We now use the relationship

$$C_b = 0.26 (L_r^*)^{-1} \tag{8}$$

deduced from the blowing experiment of Lorite-Díez *et al.* [7] plotted in Fig. 2(b). As for these data the steady asymmetric mode is observed [7] at all measured recirculation lengths, it provides the base suction $C_b^A = 0.26 (L_r^{A*})^{-1}$ with L_r^{A*} given in Eq. (5). The model is plotted in Fig. 4(a) with a blue dashed line using a best fit of the three first data points to compute the constant L_{r0}^A. There is a reasonable match but the prediction of the antisymmetric model deviates significantly from the experimental data for filling coefficient $R_f \geqslant 50\%$. The antisymmetric model overestimates the base suction or

equivalently underestimates the bubble length. This effect can reasonably be ascribed to the change of in-flux ψ_{in} at the bubble closure. To get an estimate of this change, we proceed identically for the symmetric model, assuming that Eq. (8) is also valid. Actually, Fig. 2(b) suggests that the relationship Eq. (8) is insensitive to all techniques that modify the bubble length. It is likely that through the stabilization of the steady asymmetric mode, the bubble elongates due to the in-flux increase, thus modifying the streamline curvatures after separation leading to the base suction change. It seems that Eq. (8) accounts for this global change. The symmetric model $C_b^S = 0.26 (L_r^{S*})^{-1}$ with L_r^{S*} given in Eq. (7) is plotted in Fig. 4(a) with a blue continuous line using a best fit of the two last data points to compute the constant L_{r1}^A. The two models are made to capture the jump in C_b which can now be related to the change of in flux at the bubble closure between ψ_{in}^A and ψ_{in}^S in Eq. (4) and Eq. (6). The relative in-flux change of the stabilized symmetric wake compared to that of the antisymmetric wake can be simply computed by:

$$\frac{\psi_{\text{in}}^S - \psi_{\text{in}}^A}{\psi_{\text{in}}^A} = \frac{L_{r1}^S - d - L_{r0}^A}{L_{r0}^A} = C_{b0}^A \left(\frac{1}{C_{b0}^S} - \frac{1}{C_{b0}^A} \right) = 11.6\%, \tag{9}$$

where we recall that subscripts 0 and 1 refer respectively to values at $R_f = 0$ (natural case) and $R_f = 100\%$ (plain cavity). The bubble closure of the natural wake featuring the steady asymmetric mode is more impermeable than the stabilized symmetric wake. The modeling shows that the symmetric wake in-flux is increased by 11.6% compared to the antisymmetric wake. The modeling also provides the gain in base suction reduction due to the stabilization of the steady asymmetric mode for the blunt body (i.e., $R_f = 0$):

$$\frac{C_{b0}^S - C_{b0}^A}{C_{b0}^A} = 10.4\%. \tag{10}$$

The value is in line with observations of Haffner [43] showing a base suction reduction of 8% when the wake becomes symmetric while switching between the asymmetric wake states during the stochastic bistable dynamics.

B. Ventilated base cavities

The rear slitted cavity investigated in this work is reminiscent of past studies on ventilated rear cavities [9,35], a well-known passive device to reduce the drag of blunt bluff bodies. When rear cavities are slotted and not slitted, there are walls over the whole rim of the cavity trailing edge. It initiates a flow separation as displayed by the red line in Fig. 7(a) forming the recirculating bubble. As the interior of the cavity is a low-pressure region, some external flow penetrates the cavity through the slots with a flux q_b [depicted with the thick line in Fig. 7(a)] thus producing the same effect as the base bleed on the recirculating bubble. In this case, the equivalent source q_m as defined above becomes

$$q_m = v_e l R_f d + q_b. \tag{11}$$

Depending on the value of q_b, the flux q_m can be larger with a ventilated cavity $R_f \neq 1$ than with a plain cavity with $R_f = 1$. In that case, the ventilated cavity produces a larger drag reduction that the plain cavity of identical depth. This effect first investigated for axysimmetric blunt bodies [35] is reported
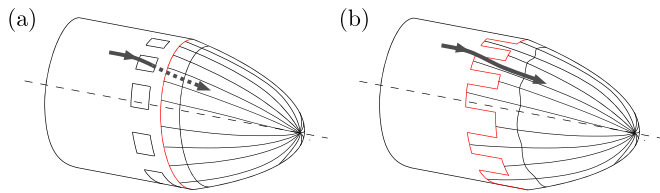
FIG. 7. Schematic drawing inspired from Délery [44] of the mean separated bubble at the rear of an axisymmetric body with a slotted (a) or slitted (b) cavity. The red line locates the separation at the trailing edge that initiates the bubble formation. The thick lines represents some external flow which may (a) or not (b) penetrate inside the bubble.

by Howell *et al.* [43] for the squareback Ahmed body. For slitted cavities, the external flux penetrating the slits remains outside the bubble as illustrated in Fig. 7(a) such that $q_b = 0$ and the beneficial effect is restricted to the mitigation of the entrainmemt flux only as described in the previous Sec. IV A.

V. CONCLUSION

Well-known drag reduction strategies using base cavities are revisited with slitted base cavities of variable filling ratios on a squareback Ahmed body. The formation length model of Gerrard [1] provides new insight of the drag mechanism.

Indeed, the adaptation of this model by Lorite-Díez *et al.* [7] to base drag prediction with base bleed control extends satisfactorily to plain or ventilated base cavities. Above all, the change of in-flux at the bubble closure has been quantified when the observed antisymmetric steady wake mode is stabilized towards a symmetric mode. This change is responsible for a base suction reduction of about 10%. The approach also demonstrates the importance of the volumetric flux budget across the vortex formation region for the pressure drag of bluff bodies in general.

Future work will attempt to investigate these fluxes using time resolved PIV and to relate them to base pressure and near wake dynamics. As the three-dimensional structure of the formation region makes the identification of these fluxes particularly challenging, complementary numerical simulations will be also considered.

[1] J. Gerrard, The mechanics of the formation region of vortices behind bluff bodies, J. Fluid Mech. **25**, 401 (1966).

[2] H. Schlichting and K. Gersten, *Boundary-Layer Theory* (Springer, Berlin, 2016).

[3] A. Roshko, Perspectives on bluff body aerodynamics, J. Wind Eng. Industr. Aerodynam. **49**, 79 (1993).

[4] P. Bearman, On vortex shedding from a circular cylinder in the critical Reynolds number regime, J. Fluid Mech. **37**, 577 (1969).

[5] P. W. Bearman, The effect of base bleed on the flow behind a two-dimensional model with a blunt trailing edge, Aeronaut. Quart. **18**, 207 (1967).

[6] T. Wu, Cavity and wake flows, Annu. Rev. Fluid Mech. **4**, 243 (1972).

[7] M. Lorite-Díez, J. I. Jiménez-González, L. Pastur, C. Martínez-Bazán, and O. Cadot, Experimental analysis of the effect of local base blowing on three-dimensional wake modes, J. Fluid Mech. **883**, A53 (2020).

[8] S. Ahmed, G. Ramm, and G. Faltin, Some salient features of the time-averaged ground vehicle wake, SAE Technical Paper 840300 (1984), https://doi.org/10.4271/840300.

[9] P. Viswanath, Flow management techniques for base and afterbody drag reduction, Progr. Aerosp. Sci. **32**, 79 (1996).

[10] M. Grandemange, M. Gohlke, and O. Cadot, Turbulent wake past a three-dimensional blunt body. part 2. experimental sensitivity analysis, J. Fluid Mech. **752**, 439 (2014).

[11] A. Evrard, O. Cadot, V. H. D. Ricot, R. Vigneron, and J. Délery, Fluid force and symmetry breaking modes of a 3d bluff body with a base cavity, J. Fluids Struct. **61**, 99 (2016).

[12] J.-M. Lucas, O. Cadot, V. Herbert, S. Parpais, and J. Délery, A numerical investigation of the asymmetric wake mode of a

squareback ahmed body—Effect of a base cavity, J. Fluid Mech. **831**, 675 (2017).

[13] M. Grandemange, O. Cadot, A. Courbois, V. Herbert, D. Ricot, T. Ruiz, and R. Vigneron, A study of wake effects on the drag of the ahmed's squareback model at the industrial scale, J. Wind Eng. Industr. Aerodynam. **145**, 282 (2015).

[14] M. Lorite-Díez, J. I. Jiménez-González, L. Pastur, O. Cadot, and C. Martínez-Bazán, Drag reduction of three-dimensional bodies by base blowing with various gas densities, Phys. Rev. E **102**, 011101(R) (2020).

[15] E.-C. Hsu, L. Pastur, O. Cadot, and V. Parezanović, A fundamental link between steady asymmetry and separation length in the wake of a 3d square-back body, Exp. Fluids **62**, 95 (2021).

[16] D. Barros, J. Borée, B. Noack, A. Spohn, and T. Ruiz, Bluff body drag manipulation using pulsed jets and coanda effect, J. Fluid Mech. **805**, 422 (2016).

[17] M. Grandemange, V. Parezanović, M. Gohlke, and O. Cadot, On experimental sensitivity analysis of the turbulent wake from an axisymmetric blunt trailing edge, Phys. Fluids **24**, 035106 (2012).

[18] G. Rigas, A. Oxlade, A. Morgans, and J. Morrison, Low-dimensional dynamics of a turbulent axisymmetric wake, J. Fluid Mech. **755**, R5 (2014).

[19] G. Rigas, A. Morgans, R. D. Brackston, and J. Morrison, Diffusive dynamics and stochastic models of turbulent axisymmetric wakes, J. Fluid Mech. **778**, R2 (2015).

[20] V. Gentile, F. Schrijer, B. Van Oudheusden, and F. Scarano, Low-frequency behavior of the turbulent axisymmetric near-wake, Phys. Fluids **28**, 065102 (2016).

[21] V. Gentile, B. Van Oudheusden, F. Schrijer, and F. Scarano, The effect of angular misalignment on low-frequency axisymmetric wake instability, J. Fluid Mech. **813**, R3 (2017).

[22] G. Pavia, M. Varney, M. Passmore, and M. T. Almond, Three dimensional structure of the unsteady wake of an axisymmetric body, Phys. Fluids **31**, 025113 (2019).

[23] T. Zhu and J. F. Morrison, Simulation of the turbulent axisymmetric bluff body wake with pulsed jet forcing, Phys. Rev. Fluids **6**, 124604 (2021).

[24] M. Grandemange, M. Gohlke, and O. Cadot, Turbulent wake past a three-dimensional blunt body. part 1. global modes and bi-stability, J. Fluid Mech. **722**, 51 (2013).

[25] R. Volpe, P. Devinant, and A. Kourta, Experimental characterization of the unsteady natural wake of the full-scale square back Ahmed body: flow bi-stability and spectral analysis, Exp. Fluids **56**, 99 (2015).

[26] R. D. Brackston, J. García De La Cruz, A. Wynn, G. Rigas, and J. F. Morrison, Stochastic modelling and feedback control of bistability in a turbulent bluff body wake, J. Fluid Mech. **802**, 726 (2016).

[27] R. D. Brackston, A. Wynn, and J. F. Morrison, Modelling and feedback control of vortex shedding for drag reduction of a turbulent bluff body wake, Int. J. Heat Fluid Flow **71**, 127 (2018).

[28] G. Pavia, M. A. Passmore, M. Varney, and G. Hodgson, Salient three-dimensional features of the turbulent wake of a simplified square-back vehicle, J. Fluid Mech. **888**, A33 (2020).

[29] Y. Fan, C. Xia, S. Chu, Z. Yang, and O. Cadot, Experimental and numerical analysis of the bi-stable turbulent wake of a rectangular flat-backed bluff body, Phys. Fluids **32**, 105111 (2020).

[30] B. Podvin, S. Pellerin, Y. Fraigneau, G. Bonnavion, and O. Cadot, Low-order modelling of the wake dynamics of an ahmed body, J. Fluid Mech. **927**, R6 (2021).

[31] D. Fabre, F. Auguste, and J. Magnaudet, Bifurcations and symmetry breaking in the wake of axisymmetric bodies, Phys. Fluids **20**, 051702 (2008).

[32] Y. Bury and T. Jardin, Transitions to chaos in the wake of an axisymmetric bluff body, Phys. Lett. A **376**, 3219 (2012).

[33] O. Marquet and M. Larsson, Global wake instabilities of low aspect-ratio flat-plates, Eur. J. Mech. B/Fluids **49**, 400 (2014).

[34] G. A. Zampogna and E. Boujo, From thin plates to Ahmed bodies: Linear andweakly non-linear stability of rectangular prisms, J. Fluid Mech. **966**, A19 (2023).

[35] T. Morel, Effect of base cavities on the aerodynamic drag of an axisymmetric cylinder, Aeronaut. Quart. **30**, 400 (1979).

[36] M. Lorite-Diez, J. Jimenez-Gonzalez, L. Pastur, O. Cadot, and C. Martinez-Bazan, Drag reduction on a three-dimensional blunt body with different rear cavities under cross-wind conditions, J. Wind Eng. Industr. Aerodynam. **200**, 104145 (2020).

[37] E. Sanmiguel-Rojas, J. I. Jimenez-Gonzalez, P. Bohorquez, G. Pawlak, and C. Martinez-Bazan, Effect of base cavities on the stability of the wake behind slender blunt-based axisymmetric bodies, Phys. Fluids **23**, 114103 (2011).

[38] M. Varney, Base Drag Reduction for Squareback Road Vehicles, Ph.D. thesis, Loughborough University, 2020.

[39] Y. Fan, V. Parezanović, and O. Cadot, Wake transitions and steady z-instability of an ahmed body in varying flow conditions, J. Fluid Mech. **942**, A22 (2022).

[40] G. Bonnavion and O. Cadot, Unstable wake dynamics of rectangular flat-backed bluff bodies with inclination and ground proximity, J. Fluid Mech. **854**, 196 (2018).

[41] C. Williamson, Vortex dynamics in the cylinder wake, Annu. Rev. Fluid Mech. **28**, 477 (1996).

[42] M. Kiya and Y. Abe, Turbulent elliptic wakes, J. Fluids Struct. **13**, 1041 (1999).

[43] J. Howell, D. Sims-Williams, A. Sprot, F. Hamlin, and R. Dominy, Bluff body drag reduction with ventilated base cavities, SAE Int. J. Passeng. Cars - Mech. Syst. **5**, 152 (2012).

[44] J. Délery, *Topologie des écoulements tridimensionnels décollés* (Lavoisier, Paris, 2013).